Analytical model and experimental verification of the critical power for modulation instability in optical fibers

Mehdi Alem,* Marcelo A. Soto, and Luc Thévenaz

EPFL Swiss Federal Institute of Technology, Institute of Electrical Engineering, Group for Fiber Optics, SCI STI LT, Station 11, CH-1015, Lausanne, Switzerland
**mehdi.alem@epfl.ch*

Abstract: Modulation instability is thoroughly investigated and a simple analytical model for its power critically modifying the wave properties in terms of system parameters is derived and experimentally validated. The differences on the modulation instability gain spectrum in lossless and lossy optical fibers are analyzed based on theoretical models and numerical simulations. In particular the impact of background noise on the behavior of modulation instability is studied analytically and verified by measurements and simulations. The proposed analytical model is experimentally validated by monitoring the wave propagation along an optical fiber using a Brillouin optical time-domain analyzer. This way, the evolution of the optical signal traveling through optical fibers, especially, the pump depletion and the recurrence phenomenon are investigated.

OCIS codes: (060.2310) Fiber optics; (060.4370) Nonlinear optics, fibers; (060.2370) Fiber optics sensors; (190.3100) Instabilities and chaos; (190.3270) Kerr effect; (290.5900) Scattering, stimulated Brillouin.

References and links

1. G. P. Agrawal, *Nonlinear Fiber Optics*, 4th ed. (Academic, 2006).
2. A. Hasegawa, "Generation of a train of soliton pulses by induced modulational instability in optical fibers," Opt. Lett. **9**(7), 288–290 (1984).
3. J. C. Travers, "Continuous wave supercontinuum generation," in *Supercontinuum Generation in Optical Fibers*, J. M. Dudley and J. R. Taylor, eds. (Cambridge University, 2010), Chap. 8.
4. K. Tai, A. Tomita, J. L. Jewell, and A. Hasegawa, "Generation of subpicosecond solitonlike optical pulses at 0.3 THz repetition rate by induced modulational instability," Appl. Phys. Lett. **49**(5), 236 (1986).
5. A. Hasegawa and W. F. Brinkman, "Tunable coherent IR and FIR sources utilizing modulational instability," IEEE J. Quantum Electron. **16**(7), 694–697 (1980).
6. K. Tai, A. Hasegawa, and A. Tomita, "Observation of modulational instability in optical fibers," Phys. Rev. Lett. **56**(2), 135–138 (1986).
7. H. Itoh, G. M. Davis, and S. Sudo, "Continuous-wave-pumped modulational instablity in an optical fiber," Opt. Lett. **14**(24), 1368–1370 (1989).
8. S. Trillo and S. Wabnitz, "Dynamics of the nonlinear modulational instability in optical fibers," Opt. Lett. **16**(13), 986–988 (1991).
9. G. Cappellini and S. Trillo, "Third-order three-wave mixing in single-mode fibers: exact solutions and spatial instability effects," J. Opt. Soc. Am. B **8**(4), 824–838 (1991).
10. J. M. Dudley, G. Genty, F. Dias, B. Kibler, and N. Akhmediev, "Modulation instability, Akhmediev Breathers and continuous wave supercontinuum generation," Opt. Express **17**(24), 21497–21508 (2009).
11. M. Erkintalo, G. Genty, B. Wetzel, and J. M. Dudley, "Akhmediev breather evolution in optical fiber for realistic initial conditions," Phys. Lett. A **375**(19), 2029–2034 (2011).
12. K. Hammani, B. Wetzel, B. Kibler, J. Fatome, C. Finot, G. Millot, N. Akhmediev, and J. M. Dudley, "Spectral dynamics of modulation instability described using Akhmediev breather theory," Opt. Lett. **36**(11), 2140–2142 (2011).
13. J. M. Dudley, F. Dias, M. Erkintalo, and G. Genty, "Instabilities, breathers and rogue waves in optics," Nat. Photonics **8**(10), 755–764 (2014).
14. B. Kibler, J. Fatome, C. Finot, G. Millot, F. Dias, G. Genty, N. Akhmediev, and J. M. Dudley, "The Peregrine soliton in nonlinear fibre optics," Nat. Phys. **6**(10), 790–795 (2010).

#248690 Received 31 Aug 2015; revised 14 Oct 2015; accepted 28 Oct 2015; published 3 Nov 2015

15. D. Anderson and M. Lisak, "Modulational instability of coherent optical-fiber transmission signals," Opt. Lett. **9**(10), 468–470 (1984).
16. Y. Chen and A. W. Snyder, "Four-photon parametric mixing in optical fibers: effect of pump depletion," Opt. Lett. **14**(1), 87–89 (1989).
17. G. P. Agrawal, "Modulation instability induced by cross-phase modulation," Phys. Rev. Lett. **59**(8), 880–883 (1987).
18. G. P. Agrawal, P. L. Baldeck, and R. R. Alfano, "Modulation instability induced by cross-phase modulation in optical fibers," Phys. Rev. A **39**(7), 3406–3413 (1989).
19. P. D. Drummond, T. A. B. Kennedy, J. M. Dudley, R. Leonhardt, and J. D. Harvey, "Cross-phase modulational instability in high-birefringence fibers," Opt. Commun. **78**(2), 137–142 (1990).
20. J. E. Rothenberg, "Modulational instability for normal dispersion," Phys. Rev. A **42**(1), 682–685 (1990).
21. K. Tajima, "Self-amplitude modulation in PSK coherent optical transmission systems," J. Lightwave Technol. **4**(7), 900–904 (1986).
22. A. Hasegawa and K. Tai, "Effects of modulational instability on coherent transmission systems," Opt. Lett. **14**(10), 512–513 (1989).
23. B. Hermansson and D. Yevick, "Modulational instability effects in PSK modulated coherent fiber systems and their reduction by optical loss," Opt. Commun. **52**(2), 99–102 (1984).
24. M. N. Alahbabi, Y. T. Cho, T. P. Newson, P. C. Wait, and A. H. Hartog, "Influence of modulation instability on distributed optical fiber sensors based on spontaneous Brillouin scattering," J. Opt. Soc. Am. B **21**(6), 1156–1160 (2004).
25. D. Alasia, M. González-Herráez, L. Abrardi, S. Martin-López, and L. Thévenaz, "Detrimental effect of modulation instability on distributed optical fiber sensors using stimulated Brillouin scattering," Proc. SPIE **5855**, 587–590 (2005).
26. S. M. Foaleng and L. Thévenaz, "Impact of Raman scattering and modulation instability on the performances of Brillouin sensors," Proc. SPIE **7753**, 77539V (2011).
27. M. A. Soto and L. Thévenaz, "Modeling and evaluating the performance of Brillouin distributed optical fiber sensors," Opt. Express **21**(25), 31347–31366 (2013).
28. H. F. Martins, S. Martin-Lopez, P. Corredera, P. Salgado, O. Frazão, and M. González-Herráez, "Modulation instability-induced fading in phase-sensitive optical time-domain reflectometry," Opt. Lett. **38**(6), 872–874 (2013).
29. Y. Dong and X. Bao, "High spatial resolution and long-distance BOTDA using differential Brillouin gain in a dispersion shifted fiber," Proc. SPIE **7503**, 750384 (2009).
30. T. Horiguchi and M. Tateda, "BOTDA-Nondestructive measurement of single-mode optical fiber attenuation characteristics using Brillouin interaction: theory," J. Lightwave Technol. **7**(8), 1170–1176 (1989).
31. T. Horiguchi, K. Shimizu, T. Kurashima, M. Tateda, and Y. Koyamada, "Development of a distributed sensing technique using Brillouin scattering: optical fiber sensors," J. Lightwave Technol. **13**(7), 1296–1302 (1995).
32. M. E. Marhic, *Fiber Optical Parametric Amplifiers, Oscillators and Related Devices* (Cambridge University, 2008).
33. M. Erkintalo, K. Hammani, B. Kibler, C. Finot, N. Akhmediev, J. M. Dudley, and G. Genty, "Higher-order modulation instability in nonlinear fiber optics," Phys. Rev. Lett. **107**(25), 253901 (2011).
34. M. Karlsson, "Modulational instability in lossy optical fibers," J. Opt. Soc. Am. B **12**(11), 2071–2077 (1995).
35. A. Carena, V. Curri, R. Guadino, P. Poggiolini, and S. Benedetto, "New analytical results on fiber parametric gain and its effects on ASE noise," IEEE Photon. Technol. Lett. **9**(4), 535–537 (1997).
36. M. E. Marhic, V. Curri, and L. G. Kazovsky, "Bessel function solution for the gain of one-pump fiber optical parametric amplifier," in *Proceedings of IEEE Conference on Nonlinear Optics* (IEEE, 1998), pp. 221–223.
37. S. Roy, M. Santagiustina, A. Willinger, G. Eisenstein, S. Combrié, and A. De Rossi, "Parametric gain and conversion efficiency in nanophotonic waveguides with dispersive propagation coefficients and loss," J. Lightwave Technol. **32**(6), 1177–1182 (2014).
38. R. G. Smith, "Optical power handling capacity of low loss optical fibers as determined by stimulated Raman and brillouin scattering," Appl. Opt. **11**(11), 2489–2494 (1972).
39. E. Fermi, J. Pasta, and H. C. Ulam, "Studies of nonlinear problems," in *Collected Papers of Enrico Fermi*, E. Segrè, ed. (University of Chicago, 1965), Vol. 2, pp. 977–988.
40. G. Van Simaeys, P. Emplit, and M. Haelterman, "Experimental demonstration of the Fermi-Pasta-Ulam recurrence in a modulationally unstable optical wave," Phys. Rev. Lett. **87**(3), 033902 (2001).
41. G. Van Simaeys, P. Emplit, and M. Haelterman, "Experimental study of the reversible behavior of modulational instability in optical fibers," J. Opt. Soc. Am. B **19**(3), 477–486 (2002).
42. A. Mussot, A. Kudlinski, M. Droques, P. Szriftgiser, and N. Akhmediev, "Fermi-Pasta-Ulam recurrence in nonlinear fiber optics: the role of reversible and irreversible losses," Phys. Rev. X **4**(1), 011054 (2014).
43. C. McKinstrie, M. Yu, M. G. Raymer, and S. Radic, "Quantum noise properties of parametric processes," Opt. Express **13**(13), 4986–5012 (2005).
44. R. Nissim, A. Pejkic, E. Myslivets, B. P. Kuo, N. Alic, and S. Radic, "Ultrafast optics. Ultrafast optical control by few photons in engineered fiber," Science **345**(6195), 417–419 (2014).
45. E. Brainis, D. Amans, and S. Massar, "Scalar and vector modulation instabilities induced by vacuum fluctuations in fibers: numerical study," Phys. Rev. A **71**(2), 023808 (2005).

#248690 Received 31 Aug 2015; revised 14 Oct 2015; accepted 28 Oct 2015; published 3 Nov 2015

46. S. M. Kobtsev and S. V. Smirnov, "Influence of noise amplification on generation of regular short pulse trains in optical fibre pumped by intensity-modulated CW radiation," Opt. Express **16**(10), 7428–7434 (2008).
47. W. Chen, Z. Meng, H. J. Zhou, and H. Luo, "Spontaneous and induced modulation instability in the presence of broadband spectra caused by the amplified spontaneous emission," Laser Phys. **22**(8), 1305–1309 (2012).
48. M. A. Soto, M. Alem, W. Chen, and L. Thévenaz, "Mitigating modulation instability in Brillouin distributed fibre sensors," Proc. SPIE **8794**, 87943J (2013).
49. M. Alem, M. A. Soto, and L. Thévenaz, "Modelling the depletion length induced by modulation instability in distributed optical fibre sensors," Proc. SPIE **9157**, 91575S (2014).
50. A. E. Ismagulov, S. A. Babin, E. V. Podivilov, M. P. Fedoruk, I. S. Shelemba, and O. V. Shtyrina, "Modulation instability of narrow-band nanosecond pulses propagating in anomalous-dispersion fibre," Quantum Electron. **39**(8), 765–769 (2009).
51. S. A. Babin, A. E. Ismagulov, E. V. Podivilov, M. P. Fedoruk, I. S. Shelemba, and O. V. Shtyrina, "Modulation instability at propagation of narrowband 100-ns pulses in optical fibers of various types," Laser Phys. **20**(2), 334–340 (2010).
52. G. B. Arfken, H. J. Weber, and F. E. Harris, *Mathematical Methods for Physics: A Comprehensive Guide* (Academic, 2013).
53. F. Alishahi, A. Vedadi, M. A. Shoaie, M. A. Soto, A. Denisov, K. Mehrany, L. Thévenaz, and C. S. Brès, "Power evolution along phase-sensitive parametric amplifiers: an experimental survey," Opt. Lett. **39**(21), 6114–6117 (2014).
54. L. Thévenaz, S. F. Mafang, and J. Lin, "Effect of pulse depletion in a Brillouin optical time-domain analysis system," Opt. Express **21**(12), 14017–14035 (2013).
55. C. Vinegoni, M. Wegmuller, and N. Gisin, "Measurements of the nonlinear coefficient of standard, SMF, DSF, and DCF fibers using a self-aligned interferometer and a Faraday mirror," IEEE Photon. Technol. Lett. **13**(12), 1337–1339 (2001).
56. A. Kobyakov, M. Mehendale, M. Vasilyev, S. Tsuda, and A. F. Evans, "Stimulated Brillouin scattering in Raman-pumped fibers: a theoretical approach," J. Lightwave Technol. **20**(8), 1635–1643 (2002).
57. A. Kobyakov, S. A. Darmanyan, and D. Q. Chowdhury, "Exact analytical treatment of noise initiation of SBS in the presence of loss," Opt. Commun. **260**(1), 46–49 (2006).

1. Introduction

Optical fibers provide ideal conditions for the observation of optical nonlinear phenomena thanks to their high energy confinement, long-range guidance and low attenuation [1]. Among the different nonlinearities occurring in an optical fiber, modulation instability (MI) has interesting features that relate it to a broad range of phenomena, from producing soliton pulses [2] to supercontinuum generation [3], while being a limitation for several applications since it substantially alters the spectrum of an optical wave [1]. Modulation instability is the break-up of an intense optical wave propagating in a nonlinear dispersive medium to a train of soliton-like pulses originating from residual minute modulations caused by intensity fluctuations [4]. MI in optical fibers has been investigated theoretically by Hasegawa and Brinkman [5] and was observed for the first time using a mode-locked pulse laser by Tai *et al*. [6] in 1985. Later, MI in a continuous-wave (CW) pump condition was observed by Itoh *et al.* in 1989 [7]. In terms of spectrum, MI generates two symmetric spectral sidebands around the pump wavelength, leading to a power exchange between pump and sidebands during the propagation along the fiber [6].

The theoretical approach to modulation instability can be based on either analyzing a four-wave mixing (FWM) framework or solving the nonlinear Schrödinger equation (NLSE). In the FWM method the pump depletion is taken into account; however, the analytic solution for most cases is not available [8,9]. The general approach to the NLSE that provides exact analytical solutions for the temporal evolution of optical pulses propagating in a dispersive Kerr medium is the Akhmediev breather formalism [10,11]. This formalism addresses the issues of pump depletion [12] and recurrence phenomenon [13] and can be effectively utilized to describe rogue waves and solitons in nonlinear fiber optics [13,14]. Another approach to the NLSE can be carried out by applying a linear stability analysis to the nonlinear equation [5]. In this method, a tiny perturbation modulates the steady-state or stationary CW solution of the NLSE, and its evolution along the fiber is investigated by linearizing the nonlinear equation considering weak perturbations with respect to the CW solution [1,15]. Since the NLSE is linearized, pump depletion can be neglected, giving rise to an undepleted

#248690 Received 31 Aug 2015; revised 14 Oct 2015; accepted 28 Oct 2015; published 3 Nov 2015

approximation that has the advantage of providing closed-form solutions for gain spectrum [1], thus giving a better insight to the behavior of modulation instability. The approximate solution of the NLSE under undepleted regime is especially appropriate for conditions in which there are no multiple optical tones interacting coherently together [16], as it is the case of having only noise-seeded modulation instability; hence the NLSE analysis will be retained for this work.

Although modulation instability can occur in normal dispersion regime due to the cross-phase modulation (XPM) between two wavelengths [17,18] or orthogonal polarizations in high-birefringence fibers [19,20], it is widely known that the NLSE for single pump in normal dispersion is stable and no MI occurs [1]. On the contrary, anomalous dispersion along with self-phase modulation (SPM) provides instability for any temporal signal in a relatively wide spectral band around the pump wavelength [6]. Therefore, most of standard optical fibers having anomalous dispersion in the telecom window of 1550 nm are subject to modulation instability. Hence, MI can affect the performance of a broad range of fiber-optic systems, such as optical communication systems, optical signal processing methods, or distributed fiber sensors, among others. For instance, it has been shown that MI degrades the signal-to-noise ratio (SNR) of coherent optical communications [15], and limits the maximum transmission distance attainable at a given bit rate [21]. In coherent transmission systems, the spectral content of modulated signals falls in the MI bandwidth and experiences a nonlinear distortion, thus imposing a severe limitation on the transmission speed of coherent systems [22]. In the particular case of optical transmission systems employing phase-shift keying (PSK) modulation format, MI can lead to a substantial distortion of the initial PSK pulse shape limiting the performance of the coherent detection process [23].

Furthermore, modulation instability has detrimental effects on different types of distributed optical fiber sensors, imposing a fundamental limit to their maximum sensing distance. In distributed fiber sensors, a high optical power must be launched into the sensing fiber to compensate the fiber attenuation and to achieve a sufficient SNR at the most remote sensing distance. However, increasing the pump power above a critical level induces fiber nonlinearities, depleting the pump power and distorting the sensor response. For instance, in Brillouin optical time-domain reflectometry (BOTDR), MI contaminates the detected signal inducing an upward offset in the measured Brillouin frequency shift (BFS) that biases the extracted temperature or strain along the fiber [24]. On the other hand, in Brillouin optical time-domain analysis (BOTDA) distributed fiber sensors, MI and stimulated Raman scattering (SRS) deplete the pump power [25,26], abruptly dropping the gain of stimulated Brillouin scattering (SBS) and hence degrading the sensor performance [27]. Furthermore, a reduction of visibility is induced in phase-sensitive optical time-domain reflectometry (ϕOTDR) by modulation instability, leading to loss of sensitivity at certain sensing positions [28]. Although utilizing dispersion shifted fibers (DSF) with normal dispersion in distributed sensing prevents modulation instability [29], most of existing fiber networks use standard SMFs and replacing them by DSFs would be too costly. It also turns out that using DSFs enhances other nonlinear effects, such as Raman scattering and FWM, due to the reduced effective area and lower dispersion favoring phase matching when compared to standard SMFs.

The purpose of this article is to analyze the behavior of modulation instability in fiber-optic systems and to propose a simple mathematical model that provides an analytical equation to the longitudinal evolution of MI in optical fibers. This explicit expression provides a good insight into the MI process, being suitable for predicting MI parameters, such as its *critical power* and the corresponding *depletion length*. Compared to existing models in the state-of-the-art, the model proposed here offers a higher accuracy in estimating the MI critical power thanks to the inclusion of pump depletion and the good approximation obtained for the noise-seeded MI gain spectrum. A mathematical analysis based on the nonlinear Schrödinger equation, along with a numerical simulation using split-step Fourier method, is

#248690 Received 31 Aug 2015; revised 14 Oct 2015; accepted 28 Oct 2015; published 3 Nov 2015

presented to provide a reliable reference for the spectral gain of MI as well as for its evolution along the fiber. Comparing the results of the proposed closed-form model with those of the comprehensive numerical simulation, the high accuracy offered by the analytical model is demonstrated. The impact of background noise mainly generated by fiber amplifiers on the onset and behavior of modulation instability is also evidenced and thoroughly investigated. In order to validate the model experimentally, the longitudinal evolution of modulation instability and the consequent pump depletion have been measured using a BOTDA system [30,31]. This system measures the Brillouin gain locally originated from a pump power (i.e. at each longitudinal position) while propagates along the fiber. Since the Brillouin interaction is narrowband compared to MI, only the optical power at the pump frequency contributes to the Brillouin gain and not the power transferred to the MI sidebands. This way, information about the local pump power and eventual MI-induced pump depletion can be straightforwardly obtained from the sensor response [27,31]. The Brillouin traces measured for different levels of input power are compared with the proposed theoretical model and numerical simulations, demonstrating the accuracy of the proposed model, which can be used as a tool to analyze and evaluate modulation instability evolution in optical fibers.

2. Analytical model

2.1 Modulation instability spectrum

The evolution of any slowly-varying envelope $A(z,t)$ normalized to the input peak power P_0 along the fiber position z, and travelling with the group velocity $v_g = 1/\beta_1$, where $\tau = t - \beta_1 z$, can be described by the nonlinear Schrödinger equation as follows [1]:

$$i\frac{\partial A}{\partial z} - \frac{\beta_2}{2}\frac{\partial^2 A}{\partial \tau^2} + i\frac{\alpha}{2}A + \gamma P_0 |A|^2 A = 0, \tag{1}$$

where β_2 is the group velocity dispersion coefficient, α is the fiber power attenuation coefficient, and γ represents the nonlinear coefficient due to the Kerr effect. Similar to optical parametric amplification (OPA) [32], the modulation instability gain is obtained by applying the *linear stability analysis* on the NLSE assuming a lossless medium (see Appendix 1 for the derivation):

$$G_{\mathrm{MI}} = 1 + 2\left(\frac{\gamma P_0}{g}\right)^2 \sinh^2(gL), \tag{2}$$

where L is the fiber length and the parametric gain coefficient g is defined as:

$$g^2 = (\gamma P_0)^2 - \left(\gamma P_0 + \frac{\Delta\beta}{2}\right)^2 = -\Delta\beta\left(\gamma P_0 + \frac{\Delta\beta}{4}\right), \tag{3}$$

in which $\Delta\beta$ denotes the linear phase mismatch between the pump, signal and idler. Note that g can take a real or imaginary value, depending on the sign of the phase mismatch $\Delta\beta$. For standard SMFs at 1550 nm (window where the second order dispersion is dominant), $\Delta\beta$ can be expressed as $\beta_2\Omega^2$, where $\Omega = \omega - \omega_0$ is the frequency detuning around the pump frequency ω_0 and β_2 is negative (anomalous dispersion). This way, the following expression for the MI gain is obtained by substituting $\Delta\beta = \beta_2\Omega^2$ in Eq. (3) and then g in Eq. (2), so that:

#248690 Received 31 Aug 2015; revised 14 Oct 2015; accepted 28 Oct 2015; published 3 Nov 2015

$$G_{\mathrm{MI}}(\Omega) = 1 + \frac{\sinh^2\left(2\gamma P_0 L \sqrt{\left(\frac{\Omega}{\Omega_c}\right)^2\left(1-\left(\frac{\Omega}{\Omega_c}\right)^2\right)}\right)}{2\left(\frac{\Omega}{\Omega_c}\right)^2\left(1-\left(\frac{\Omega}{\Omega_c}\right)^2\right)}, \tag{4}$$

where the cutoff frequency Ω_c is given by:

$$\Omega_c = \sqrt{\frac{4\gamma P_0}{|\beta_2|}}. \tag{5}$$

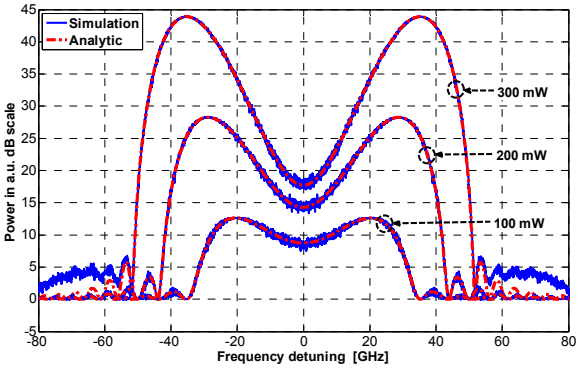

Fig. 1. MI gain spectrum for a 10 km lossless SMF with different values of input power and typical values of γ = 1.8 W^{-1}/km and β_2 = –22 ps^2/km. Comparison between simulations of the NLSE (continuous blue line) and the analytical solution according to Eq. (4) (red dashed line).

The maximum gain of the MI gain spectrum can be easily calculated from Eq. (4) as $1 + 2\sinh^2(\gamma P_0 L)$, which occurs at the frequency detuning $\pm\Omega_c/\sqrt{2}$ [1]. Although this maximum gain only depends on the input power and not on the dispersion, the MI spectral width is very sensitive to the dispersion parameter β_2 and it can be hugely increased by approaching the zero-dispersion wavelength (ZDW). Since the ZDW of standard SMFs is far away from the 1550 nm window, the impact of ZDW fluctuations on the gain spectrum can be confidently neglected [32]. Figure 1 shows the MI gain spectrum for an SMF with different levels of input power and compares numerical and analytical solutions. While analytical results (dashed red lines) are obtained directly from Eq. (4), the numerical results (continuous blue lines) have been obtained by applying a Monte Carlo simulation to the nonlinear Schrödinger equation, numerically solved by using the split-step Fourier method [1]. It is evident that the simulation and the analytical gain given in Eq. (4) are in perfect agreement. The small discrepancy between theory and simulation observed outside the main MI sidelobes, for the case of 300 mW input power is due to the higher-order modulation instability [33], which is neglected in the analytical model and only occurs with very high power levels (more than the normal power regime used in optical fiber systems). Figure 1 also shows that the gain at the pump frequency (Ω = 0) has a quadratic dependence on the pump power (note that Fig. 1 is in dB scale), which is given by $1 + 2(\gamma P_0 L)^2$ deduced from Eq. (4), while the gain at the peak frequency depends exponentially on the pump power.

It should be reminded that the gain spectrum given by Eq. (4) is valid for lossless fibers. In the case of lossy fibers, the gain can be expressed in terms of modified Bessel [34], Hankel [35], ordinary Bessel [36], or Whittaker [37] functions; all with complex-valued orders that are extremely complicated for calculation. Therefore, this motivates a modification of the lossless gain to consider the effect of the fiber loss in MI gain spectrum. A tentative

#248690 Received 31 Aug 2015; revised 14 Oct 2015; accepted 28 Oct 2015; published 3 Nov 2015

approximate expression can be obtained multiplying Eq. (2) by the attenuation factor $e^{-\alpha L}$ (α being the attenuation coefficient) and replacing the fiber length L by its corresponding effective length defined as [1,32]:

$$L_{\text{eff}} = \frac{1 - e^{-\alpha L}}{\alpha}. \tag{6}$$

This way, Eq. (2) can be expressed as:

$$G_{\text{MI}} = e^{-\alpha L}\left(1 + G_{\text{p}}\right) = e^{-\alpha L}\left(1 + 2\left(\frac{\gamma P_0}{g}\right)^2 \sin \text{h}^2\left(g L_{\text{eff}}\right)\right), \tag{7}$$

where G_{p} denotes the net gain generated by the sole pump.

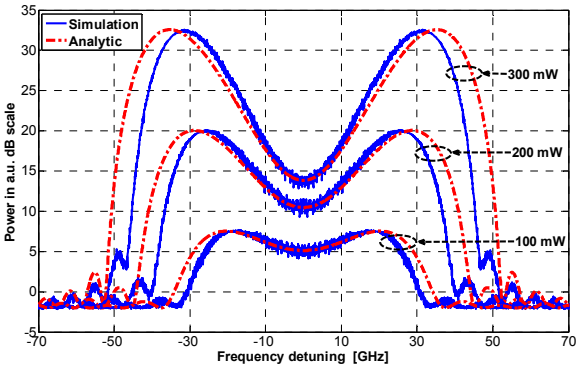

Fig. 2. MI gain spectrum for a 10 km SMF with different values of input power and typical values α = 0.2 dB/km, γ = 1.8 W^{-1}/km and β_2 = –22 ps^2/km. Note that the negative baseline level (–2 dB) is simply a consequence of the fiber loss here considered in the calculation.

Figure 2 shows the MI gain spectrum obtained by the approximated model reported in Eq. (7) (red dashed lines) and by the Monte Carlo simulation of the NLSE given in Eq. (1) (blue continuous lines). For the sake of visual clarity, the vertical axis of the figure is plotted in dB scale, highlighting clear differences in both spectrum. However, it is important to notice that the differences are only in the bandwidth of the MI gain and not in the peak gain value, which is actually the same in the two cases, being equal to $e^{-\alpha L}(1 + 2\sinh^2(\gamma P_0 L_{\text{eff}}))$. Considering that the MI gain spectrum is actually very sharp in linear scale, the integral of this spectrum (representing the energy transfer involved in the MI process) is mostly determined by the peak gain. On the other hand, the MI bandwidth obtained from Eq. (7) is slightly higher than the exact one and therefore the calculated transfer energy to the MI sidebands could be considered as an upper bound approximation. Another important aspect of this undepleted approximation is that the analytical gain slightly overestimates the level of MI (since the real depletion will reduce the actual net MI gain), and so the model provides a safe upper bound for MI in terms of power transferred into the sidebands. This is actually the same approach followed by R. G. Smith to calculate the well-known expressions for the critical powers of SRS and SBS [38].

2.2 Model of MI in the low-depletion regime

The MI gain spectra presented in Eq. (2) and Eq. (7) assume an undepleted pump condition. Therefore, the models must be prudently used for low pump depletion; otherwise using them in high depletion regime might lead to inaccurate results. However, in order to improve the accuracy of the models, here a small amount of depletion is introduced by defining a *depletion ratio*, which corresponds to the quotient between the depleted pump power $P_{\text{MI}}(z)$

#248690 Received 31 Aug 2015; revised 14 Oct 2015; accepted 28 Oct 2015; published 3 Nov 2015

and the nominal value of the pump power at a position z, i.e. $P_0e^{-\alpha z}$. Note that P_{MI} is actually the transferred power from the pump to the MI spectral sidebands due to the MI process. Considering $P(z)$ as the actual local pump power at a fiber position z, the local depletion ratio $R_D(z)$ can be expressed as follows:

$$R_D(z) \triangleq \frac{P_{MI}(z)}{P_0e^{-\alpha z}} = \frac{P_0e^{-\alpha z} - P(z)}{P_0e^{-\alpha z}} = 1 - \frac{P(z)}{P_0e^{-\alpha z}}. \quad (8)$$

To make sure that the undepleted approximation is still accurate enough when depletion is incorporated into the model, the depletion ratio must be kept low. This actually agrees with the concept of *critical power*, which corresponds to the input pump power at the *onset* of a nonlinear interaction. Since this onset always takes place in a low-depletion regime, the undepleted approximation is still valid. As it will be described later, a maximum depletion of 20% has been here considered for analysis and to compare with experimental results. This depletion ratio is still lower than the one considered when defining the critical powers for SRS and SBS [38], and can ensure an accurate description of the MI evolution along an optical fiber, as demonstrated later in Section 4.

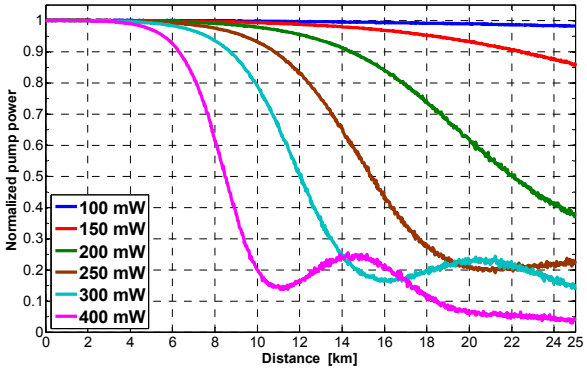

Fig. 3. Pump power evolution along an SMF of 25 km with α = 0.2 dB/km, γ = 1.8 W^{-1}/km and β_2 = –22 ps^2/km, in presence of noise with a power spectral density of –121 dBm/Hz. Note that the pump power is normalized to $P_0e^{-\alpha z}$ to discard the effect of the fiber loss on the curves.

Figure 3 depicts the longitudinal evolution of the pump power (normalized to $P_0e^{-\alpha z}$ to compensate for the fiber attenuation) along the fiber position, obtained by numerical simulation of the NLSE for different levels of input power. Besides showing pump depletion, the oscillatory behavior of the pump power propagating through the fiber is evident. This phenomenon, which is responsible for exchanging power between both pump and signal, is called Fermi-Pasta-Ulam (FPU) recurrence [39] and it has been theoretically studied and experimentally demonstrated in optical fibers [40–42]. It should be mentioned that the analytical expression of gain given in Eq. (2) cannot explain the FPU recurrence since it neglects pump depletion. This is because the partially reversible behavior of pump power becomes evident only in highly *nonlinear* regime, while the gain spectrum in Eq. (2) is obtained via *linear* stability analysis of the NLSE, which is only a first-order (linear) approximation. In contrast to the analytical solution, numerical simulations consider the whole phenomenon, showing the oscillatory evolution of pump power. However, as it is clear from Fig. 3, the FPU phenomenon occurs, as expected, in a highly depleted regime, which can be avoided by keeping the depletion ratio low in our analytical model and experimental investigation.

2.3 Impact of background noise on the evolution of MI

It is worth mentioning that modulation instability and optical parametric amplification are in essence the same process, both being originated by Kerr effect; for this reason sometimes the

#248690 Received 31 Aug 2015; revised 14 Oct 2015; accepted 28 Oct 2015; published 3 Nov 2015

two terms are interchangeably used in the literature [4,40]. However if the focus is placed on the subtle differences, it should be noticed that in OPA a deterministic signal and the background noise within the OPA spectral band [43] are amplified via energy transfer from a high-power pump to a signal and idler through a four-photon mixing process [44]. Modulation instability is however solely seeded by the background noise present in the spectral band of MI [35], so that the background noise plays the simultaneous roles of signal and idler for modulation instability; it is therefore essential to take into account the randomness inherent in noise when analyzing modulation instability. The strong impact of the background noise level on the MI evolution has been shown theoretically [45,46] and experimentally [47,48]; thus neglecting this effect would certainly lead to a discrepancy between the experimental data and any theoretical model [26].

Figure 4 shows the output pump power (normalized to $e^{-\alpha L}$, being L = 10 km of fiber length) from an SMF versus the input power, for different values of background noise in the fiber. The plots are obtained by applying the split-step Fourier method to solve the NLSE and exploiting a Monte Carlo simulation to consider the noise. In order to analyze the impact of the noise power, and the respectively seeded MI, on the output pump power, a wide range of noise levels has been considered in Fig. 4, ranging from the quantum noise level (being −161 dBm/Hz at 1550 nm) up to −101 dBm/Hz using power steps of 10 dB. The figure self-explains how strong the noise level influences the onset and behavior of MI. Results clearly point out that increasing the noise level seeds more MI; and thus, reduces the output pump power as a consequence of the increased pump depletion. Therefore, the input pump power for which MI starts to be significant crucially depends on the noise level present in the system. In the state-of-the-art, there have been some few attempts to obtain an observation threshold [26] or a depletion length [49] for MI; however, this has been limited to some specific cases only, such as when using Gaussian pulses [50,51]. In [46] an analytical formula is provided for the critical length corresponding to the distance at which pump depletion is maximal. The result has been improved using the Akhmediev breather formalism in [11]; however, their analysis is focused on the pump interaction with a single-frequency coherent signal and not on its interaction with noise over the whole MI spectral band. Therefore, a more general analysis of the critical power for the onset of MI is still missing in the literature. This is the aim of the analysis presented hereafter in this section. More specifically, Section 2.4 presents a general model for the MI critical power, which takes into account pump depletion and the noise-seeded MI gain spectrum. This way, a more accurate model for the MI critical power is obtained when compared to the models existing in the state-of-the-art, consolidated by an experimental verification.

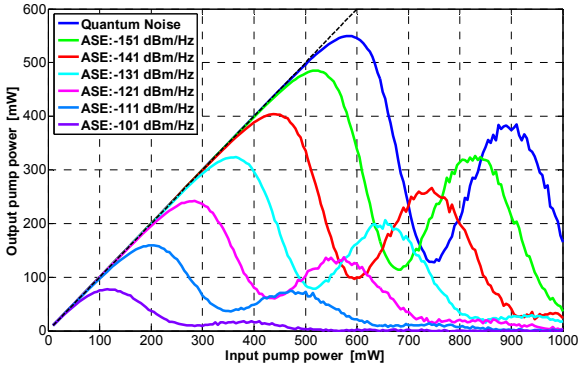

Fig. 4. Output pump power versus input power for an SMF with length L = 10 km, α = 0.2 dB/km, γ = 1.8 W^{-1}/km and β_2 = –22 ps^2/km. Note that the pump power is normalized to $e^{-\alpha L}$ to discard the effect of the fiber attenuation on the curves.

#248690 Received 31 Aug 2015; revised 14 Oct 2015; accepted 28 Oct 2015; published 3 Nov 2015

2.4 Modeling the MI critical power

In order to evaluate the MI critical power or depletion length analytically, it is necessary to calculate the power transferred from the pump into the MI spectral sidebands. However, note that the total power in the MI sidebands does not only include the power transferred from the pump, but also the input noise power. This noise power is actually independent of the pump and can be associated to the unitary term in the expression for the MI gain given in Eq. (7); whilst the net gain G_{P} is responsible for the power transferred from the pump into the MI sidebands. This transferred power can be obtained by integrating the entire MI, as follows:

$$P_{\mathrm{MI}} = \frac{e^{-\alpha L}}{2\pi}\int_0^{\infty} S_n(\omega) G_{\mathrm{P}}(\omega)\, d\omega \approx \frac{e^{-\alpha L}}{2\pi}\int_{\omega_0 - m\Omega_c}^{\omega_0 + m\Omega_c} S_n(\omega) G_{\mathrm{P}}(\omega)\, d\omega, \tag{9}$$

where $S_n(\omega)$ is the single-sided noise power spectral density (PSD) expressed in W/Hz and the positive integer m shows the number of spectral sidebands taken into account for calculating the depleted power. Since most of power is in the first side lobes of the MI symmetric spectrum, m can be set to 1 with fairly acceptable accuracy. However, the larger m the more accurate the approximation will be; ideally, m should tend to infinity.

In a real system, the main source of noise launched into optical fibers comes from the amplified spontaneous emission (ASE) generated in optical amplifiers, such as the commonly-used erbium-doped fiber amplifiers (EDFA). Since the MI spectral width is quite narrow (less than 1 nm) compared to the ASE bandwidth, the noise PSD can be assumed to be white and so independent of frequency. With that consideration, and by normalizing and centering the frequency variable through $x = \Omega/\Omega_c = (\omega - \omega_0)/\Omega_c$, and letting m go to infinity, Eq. (9) can be written as follows:

$$P_{\mathrm{MI}} = \frac{e^{-\alpha L} S_n \Omega_c}{2\pi}\lim_{m\to\infty}\int_{-m}^{m} G_{\mathrm{P}}(x)\, dx = \frac{e^{-\alpha L} S_n \Omega_c}{2\pi}\int_{-\infty}^{\infty} G_{\mathrm{P}}(x)\, dx = \frac{e^{-\alpha L} S_n \Omega_c}{\pi}\int_0^{\infty} G_{\mathrm{P}}(x)\, dx, \tag{10}$$

where the net gain is given by:

$$G_{\mathrm{P}}(x) = \frac{\sin \mathrm{h}^2\left(2\gamma P_0 L_{\mathrm{eff}}\sqrt{x^2\left(1-x^2\right)}\right)}{2x^2\left(1-x^2\right)}. \tag{11}$$

It is worth noting that $G_{\mathrm{P}}(x)$ is a real-valued even function, justifying the integration only over positive values in Eq. (10). Since the hyperbolic sine in Eq. (11) has an exponential behavior and sharp peaks at $x_0^2 = ½$, the integral in Eq. (10) can be approximated using the *steepest descent* method [52], leading to the following result (see Appendix 2 for the derivation):

$$I = \int_0^{\infty} G_{\mathrm{P}}(x)\, dx \approx \frac{e^{2\gamma P_0 L_{\mathrm{eff}}}\sqrt{\pi}}{4\sqrt{2\gamma P_0 L_{\mathrm{eff}}}}. \tag{12}$$

Substituting the integral I in Eq. (10) and using the cutoff frequency in Eq. (5), the depleted power is obtained as follows:

$$P_{\mathrm{MI}} = \frac{S_n e^{2\gamma P_0 L_{\mathrm{eff}} - \alpha L}}{2\sqrt{2\pi L_{\mathrm{eff}}\left|\beta_2\right|}}. \tag{13}$$

Considering the definition of depletion ratio given in Eq. (8), the above expression can be rewritten as follows:

$$e^{2\gamma P_0 L_{\mathrm{eff}}} = \frac{2R_{\mathrm{D}}\sqrt{2\pi L_{\mathrm{eff}}\left|\beta_2\right|}}{S_n} P_0. \tag{14}$$

#248690 Received 31 Aug 2015; revised 14 Oct 2015; accepted 28 Oct 2015; published 3 Nov 2015

Equation (14) can be seen as a transcendental equation for the input power P_0 when there is a fractional depletion R_D of the pump power. Denominating this input power as the *critical power* P_{crit} and taking the logarithm of Eq. (14), the following expression can be obtained to calculate the critical input power of modulation instability:

$$2\gamma P_{crit} L_{eff} = \ln\left(\frac{2R_D \sqrt{2\pi L_{eff} |\beta_2|}}{S_n} P_{crit} \right). \tag{15}$$

The linear gain $\sigma = 2\gamma P_0 L_{eff}$ can be defined as the exponent of the MI gain in Eq. (4) and thus the above critical power equation can be written in terms of the critical gain $\sigma_{crit} = 2\gamma P_{crit} L_{eff}$ as follows:

$$\sigma_{crit} = \ln\left(\frac{R_D \sqrt{2\pi |\beta_2|}}{S_n \gamma \sqrt{L_{eff}}} \sigma_{crit} \right). \tag{16}$$

Equation (16) has no closed-form solution and must be solved for σ_{crit} numerically to obtain the critical input power of modulation instability. In the case of standard SMFs, the typical values α = 0.2 dB/km, β_2 = –22 ps^2/km, and γ = 1.8 W^{-1}/km can be considered, together with the effective length approximated to α^{-1} = 21.7 km for long fibers. Substituting all the numerical parameters in Eq. (16) and expressing the noise power spectral density S_n in dBm/Hz instead of W/Hz, the following equation for σ_{crit} is obtained:

$$\sigma_{crit} - \ln(\sigma_{crit}) = \ln(R_D) - \left(\frac{S_n}{10} + 9 \right) \ln(10) + \frac{\ln(2)}{2}. \tag{17}$$

Figure 5 plots the critical gain σ_{crit} versus the fiber length obtained in three ways: *i*) the simulation of the NLSE, *ii*) the solution of Eq. (16), and *iii*) its approximation in Eq. (17). Two levels of ASE noise, namely –121 dBm/Hz and –141 dBm/Hz, along with two depletion ratios, i.e. 10% and 20%, are assumed in Fig. 5 to describe how σ_{crit} varies with the amount of tolerable depletion R_D and the noise power spectral density S_n.

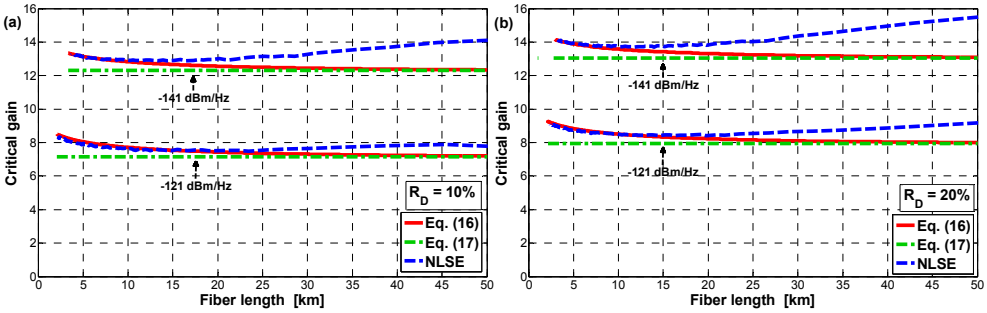

Fig. 5. Critical linear gain σ_{crit} versus fiber length obtained from the NLSE, Eq. (16) and Eq. (17) for (a) R_D = 10% and (b) R_D = 20%, using two values of noise PSD: –121 and –141 dBm/Hz. Note that the critical gain is here obtained considering that the depletion ratio of R_D occurs at the end of a given fiber, whose length ranges from 2 km up to 50 km.

As it is evident from Fig. 5, all four samples have the same behavior. In short length regime the NLSE and Eq. (16) are in good agreement since the undepleted pump approximation is accurately valid; while Eq. (17) has a discrepancy since the effective length approximation (i.e. assuming $L_{eff} = \alpha^{-1}$ = 21.7 km) is not accurate in short ranges, where L_{eff} is clearly shorter than 21.7 km. On the other hand, in long fibers the solution of the analytical model differs from the simulation of the NLSE due to the loss of accuracy of the undepleted pump approximation for long propagation lengths, which lead to more nonlinear interaction. However, Eq. (17) approximates the solution of Eq. (16) asymptotically in long distances.

#248690 Received 31 Aug 2015; revised 14 Oct 2015; accepted 28 Oct 2015; published 3 Nov 2015

Actually, it is worth noticing that the constant critical gain obtained from Eq. (17) determines in all cases a safe and relatively accurate limit on the peak power to avoid a certain amount of MI depletion, keeping in mind that the real critical power could be slightly higher for a real system. It should also be noticed that since the MI gain is here calculated from the undepleted spectral shape, the lower the depletion ratio, the more accurate the model is and thus the obtained value for σ_{crit}. This is evident when comparing Fig. 5(a) with Fig. 5(b). Since the variation of σ_{crit} with respect to fiber length turns out to be negligible when compared to the effect of other factors such as noise and tolerable depletion ratio, a critical gain σ_{crit} can be calculated with an acceptable approximation by using Eq. (17) independently from the fiber length. This way, the critical power can be calculated for any fiber length via the following expression:

$$P_{\text{crit}} = \frac{\sigma_{\text{crit}}}{2\gamma L_{\text{eff}}}. \tag{18}$$

For example, if a system tolerates a maximum depletion of 10%, i.e. $R_D = 0.1$, and the background noise level launched into the fiber is $S_n = -121$ dBm/Hz, Eq. (17) can be reduced to $\sigma_{\text{crit}} - \ln(\sigma_{\text{crit}}) = 5.18$, which gives a solution equal to $\sigma_{\text{crit}} = 7.15$. So, for a 25-km standard SMF with $\gamma = 1.8$ W^{-1}/km the critical input power that induces at most 10% of depletion at the fiber end can be simply calculated from Eq. (18) to be around 135 mW. This value actually agrees very well with experimental observation reported in the literature [48]. It should be clarified that the depletion ratio in this case is 10% only at the end of the fiber (25 km), and it is certainly lower at shorter distances along the fiber.

3. Validating setup

In order to validate the analytical model and numerical results regarding the longitudinal evolution of modulation instability, a standard BOTDA system [30] has been utilized to obtain experimental results. This system is based on a pump-probe interaction, in which a high-power pump pulse and a continuous-wave probe signal are launched into opposite ends of a fiber under test. While the high-power pump pulse induces MI in the fiber, the low-power probe signal is simply used to measure the longitudinal evolution of the pump power through Brillouin gain. Since the Brillouin gain is proportional to the pump power in the small gain approximation, the longitudinal evolution of pump pulse and any depletion induced by MI can be directly measured by analyzing the Brillouin gain affecting the probe power [53]. The scheme is sketched in Fig. 6.

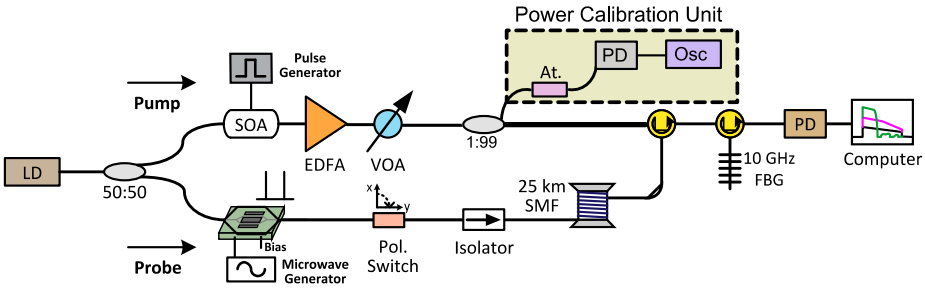

Fig. 6. Experimental setup based on a standard BOTDA scheme; LD: laser diode; SOA: semiconductor optical amplifier; EDFA: erbium-doped fiber amplifier; VOA: variable optical attenuator; FBG: fiber Bragg grating; At.: 10 dB attenuator; PD: photodetector; Osc: Oscilloscope; EOM: electric-optic modulator; SMF: single-mode fiber.

The light from a distributed feedback (DFB) laser diode (LD) at 1551.1 nm is split into pump and probe branches by a 50:50 coupler. A semiconductor optical amplifier (SOA) is used to shape pulses of 20 ns with high extinction ratio (>50 dB) and repetition period of 300

#248690 Received 31 Aug 2015; revised 14 Oct 2015; accepted 28 Oct 2015; published 3 Nov 2015

μs, longer than the return-trip time in the fiber. Pump pulses are amplified by a low-noise EDFA and attenuated by a variable optical attenuator (VOA) to precisely adjust different pump peak powers. A power calibration unit (shown in the dashed box) is used for monitoring the peak power launched into the fiber under test (FUT), which corresponds to a 25.5 km-long standard SMF. For the probe branch, an electro-optic modulator (EOM) is employed to generate a two-sideband probe with suppressed carrier, and a polarization switch is inserted to eliminate the polarization dependence of the SBS gain. An isolator in the probe branch is used to stop the pump pulses propagating back through the output of the EOM. A 10-GHz fiber Bragg grating (FBG) is employed to filter out one of the probe sidebands and the Rayleigh backscattered light from the pulses, so that only one of the probe sidebands is launched into a 125 MHz photo-detector (PD). Finally, a computer acquisition card is used to record the time-domain traces.

It is important to mention that the FUT has a very uniform Brillouin gain, ensuring that the recorded time-domain trace at a given pump-probe frequency offset is proportional to the pump power at each fiber position [27], discarding any potential effect induced by spectral variations of the Brillouin gain. This way, the acquired traces can show a reliable profile of the longitudinal evolution of the pump power along the fiber. It is also noteworthy that the probe power is kept very low in comparison with the pump power, so that the SBS-induced depletion can be safely neglected [54] and the traces only include the effect of MI. The optical fiber utilized in this experiment is a standard SMF of length 25.5 km with typical attenuation of 0.2 dB/km and anomalous GVD coefficient of −22 ps^2/km. The nonlinear coefficient of the fiber under test has been measured using a self-aligned interferometer with a Faraday mirror, as described in [55]; the measured nonlinear coefficient is 1.8 W^{-1}/km.

Figure 7 sketches two modifications in the standard BOTDA configuration to quantitatively verify the impact of ASE noise on modulation instability. In Fig. 7(a), an EDFA is used as a source of ASE noise which is coupled to the pump pulses through a 50:50 coupler. The level of noise spectral density is controlled via a variable optical attenuator. Using this configuration, the evolution of the pump power during propagation along the fiber can be investigated in presence of different levels of co-propagating background noise, seeding modulation instability at different levels.

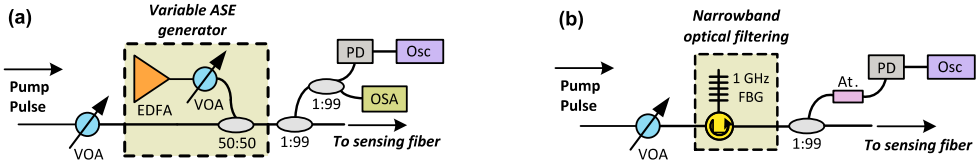

Fig. 7. Two modifications to the standard BOTDA system; used to analyze the impact of noise on the behavior of modulation instability: (a) Scheme used to couple ASE noise co-propagating with the pump pulses; (b) Scheme used to filter out ASE noise from the pump pulses.

On the other hand, Fig. 7(b) shows a configuration designed for filtering the ASE noise (within the MI spectral band) generated by the EDFA used to boost the pump pulses (see Fig. 6). The filter includes a circulator and a narrowband FBG with a bandwidth of 1 GHz. Since the spectral band of modulation instability is in the range of a few tens of GHz, the 1 GHz filter used in this configuration can filter most of the ASE noise within the MI bandwidth.

4. Experimental results

Using the BOTDA system sketched in Fig. 6, the longitudinal power evolution of an optical pulse during its propagation along an optical fiber can be obtained by measuring the local linear Brillouin amplification [27,30]. In the performed experiment, pump pulses have duration of 20 ns, corresponding to a spatial resolution of 2 m, and traces have been acquired with 2000 times averaging. The pump-probe frequency offset has been set to the average

#248690 Received 31 Aug 2015; revised 14 Oct 2015; accepted 28 Oct 2015; published 3 Nov 2015

Brillouin frequency of the fiber (10.84 GHz), so that the measured longitudinal power evolution can be mostly attributed to modulation instability and fiber attenuation (to ensure this, the Brillouin frequency of the fiber was previously measured, verifying negligible longitudinal variations).

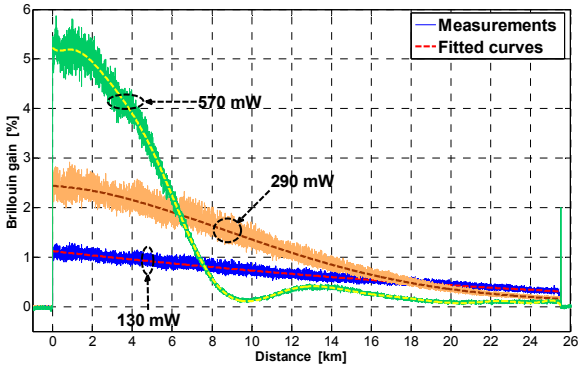

Fig. 8. Brillouin traces along with their fitted curves, for three different values of input pump power: 130 mW, 290 mW, and 570 mW.

Figure 8 shows the pulse peak power evolution along the optical fiber for three different input pump powers: 130 mW, 290 mW and 570 mW. For the case of the lowest power (130 mW), it is possible to observe the natural exponential power decay given by the fiber attenuation; however, as pulse power increases, the peak power evolution changes due to the onset of modulation instability. Comparing the curves in Fig. 8, it is interesting to notice that increasing the input power of an optical signal launched into the fiber can even decrease the signal power propagating at far distances as a consequence of the pump depletion induced by modulation instability. In other words, increasing the input power does not necessarily enhance the power propagating in the fiber at the original wavelength, but sometimes can degrade it due to nonlinear distortions, such as modulation instability. At high input power, the FPU recurrence phenomenon turns out evident, as shown by the oscillatory behavior in Fig. 8 for a pump power of 570 mW. An important aspect to mention is that, since the depletion is oscillatory it is possible to assume that MI is dominant and the depletion induced by other processes, such as SRS and SBS, is negligible. The measured longitudinal traces have been fitted to polynomial curves, as shown by the dashed lines in Fig. 8. This way, the experimental evolution of the pump power (proportional to the measured Brillouin gain) can be represented in absence of noise, thus providing a clean reference for comparing with analytical and simulation data.

In order to investigate the impact of the background noise on the onset and behavior of MI, an EDFA has been used to introduce noise into the system based on the scheme shown in Fig. 7(a). Figure 9(a) shows the longitudinal BOTDA traces obtained with an input pump power of 60 mW, for different levels of noise. Under the lowest noise situation, the time-domain BOTDA trace can be measured with no distortion; however, when the ASE noise increases, MI is seeded enough to deplete the pump. This behavior experimentally validates that the onset of modulation instability depends not only on the peak pump power (in this case kept fixed), but also on the power level of the background noise co-propagating with the pump within the MI spectral band. Figure 9(b) reports similar results, but for an input peak power of 500 mW. In this case MI substantially distorts the expected exponential decay of the pulse power along the fiber as a consequence of the high input power, even at low noise conditions. However, it is possible to observe that the presence of ASE noise further seeds MI, increasing the amount of pump depletion. The results validate the behavior described in Fig. 4 and demonstrate the key role of the noise spectrum S_n in the analytical formula proposed in Eq. (17). It is worth noting that the small negative level obtained in the calculated

#248690 Received 31 Aug 2015; revised 14 Oct 2015; accepted 28 Oct 2015; published 3 Nov 2015

gain shown in Fig. 9(b) for the PSD of −115 dBm/Hz does not have any relation to the MI evolution, but results in the measurement process simply from the uneven and limited-bandwidth response of the photo-detector.

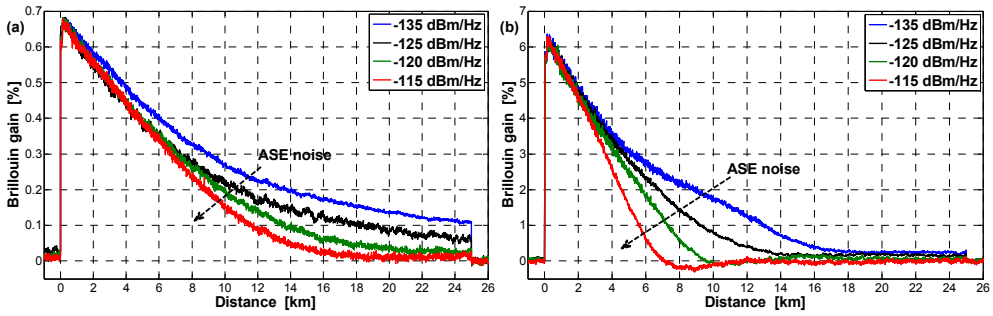

Fig. 9. Longitudinal BOTDA traces for different noise PSD values, ranging from −135 dBm/Hz up to −115 dBm/Hz, and for an input peak power of (a) 60 mW and (b) 500 mW.

A second test to verify the effect of noise on MI has been carried out employing the scheme in Fig. 7(b). In this case most of the ASE noise co-propagating with the pump pulses is filtered out, thus providing a potential reduction of the seeding of MI. Figure 10(a) shows how filtering the ASE noise within the MI spectral band changes the onset of MI and thus decreases the MI depletion. The comparison between filtered and non-filtered pump cases clearly highlights the importance of background noise in seeding MI and how filtering can mitigate its impact.

Figure 10(b) shows the Brillouin gain measured at the end of the FUT as a function of the pump power, illustrating the effect of filtering on the output pulse power. It can be observed that the amount of MI-induced depletion decreases significantly by filtering out the ASE noise in the spectral band of modulation instability. This leads to higher output pulse power (red line in the figure) with respect to the case in which the noise is not filtered out (blue line), especially for high power regime. It should be noted that the residual noise passing through the 1 GHz filter still induces some level of MI, thus inducing also some pump depletion, but at higher pump powers. This explain why the red curve in Fig. 10(b) does not follow a perfect straight line as a function of the input power, but shows a clear behavior of pump depletion. It should be emphasized that even with a perfect filter covering only the bandwidth of the propagating signal, MI will always occur if there is co-propagating noise. This is because the spectral MI gain at a $\Omega = 0$ is not null, which means that any in-band noise co-propagating along the fiber will always seed MI, inducing some level of depletion, which essentially depends on the noise PSD and bandwidth of the optical filter.

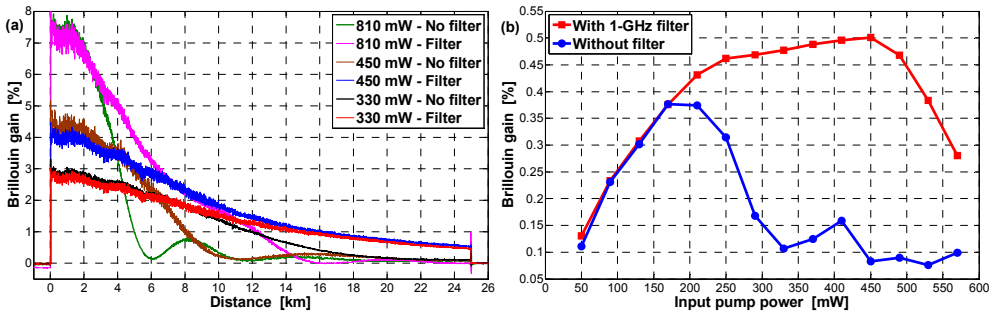

Fig. 10. (a) BOTDA traces for different peak power levels for filtered and non-filtered cases. (b) SBS gain measured in the last meters of the 25 km SMF versus input pump power, with (red squares) and without (blue circles) narrowband optical filtering.

#248690 Received 31 Aug 2015; revised 14 Oct 2015; accepted 28 Oct 2015; published 3 Nov 2015

In order to validate the proposed analytical model, theoretical results obtained from Eq. (17) are compared with both numerical simulations and experiments. The simulation is carried out by applying the split-step Fourier method to the NLSE and utilizing the Monte Carlo algorithm to take the noise into account. It should be noted that the simulation considers the MI-induced pump depletion, while the theoretical model uses the MI gain in the undepleted regime. On the other hand, in the experiment, the fiber position showing a certain depletion ratio is extracted from the measured BOTDA traces, thus obtaining the respective depletion length for different input pump powers. This way, the input pump power leading to a given depletion length corresponds to the MI critical power for a fiber of length equal to the calculated depletion length. It should be mentioned that since the peak power of pump pulses is still lower than the SRS threshold [26,38], this depletion is very certainly not caused by Raman scattering. On the other hand the pulse duration of 20 ns and thus short interaction length prevents SBS from depleting the pump at this range of peak power [38].

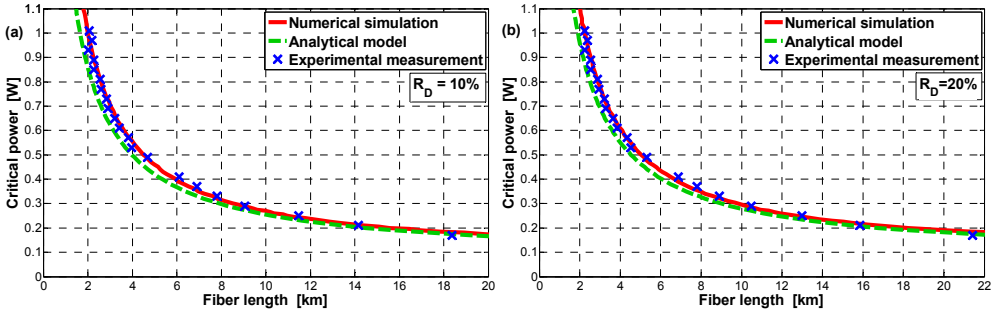

Fig. 11. Critical power P_{crit} versus fiber length obtained by numerical simulations, experimental measurements and analytical model for two depletion ratios: (a) R_D = 10% and (b) R_D = 20%.

Figure 11 depicts the critical power versus the fiber length for two depletion ratios, namely, 10% and 20%. As expected, the numerical simulations match perfectly the measurement results because in simulating the NLSE the pump depletion is taken into account. More importantly, the analytical results obtained with the proposed model follow exactly the measurements and simulations but with a small discrepancy due the undepleted regime and effective length approximations used to derive Eq. (17). Such approximations ensure that the model gives a safe critical power for modulation instability.

The critical linear gain σ_{crit} is plotted versus the fiber length in Fig. 12 for the same two depletion ratios (i.e. 10% and 20%). It should be mentioned that, compared to the behavior shown in Fig. 5, here the critical gain obtained as a function of the distance is not a straight horizontal line, but increases with distance as a consequence of the non-uniform ASE noise power used when measuring the different pump power conditions. Actually since the input power level is adjusted by a variable optical attenuator (see Fig. 6) and varied by about 10 dB, the ASE noise introduced by the EDFA is also modified in the same range, thus leading to a different behavior when compared to Fig. 5, in which a constant ASE noise was assumed. Under this condition Fig. 12 shows a good agreement between measurement, simulations and analytical solution. It is possible to observe that by increasing the tolerable depletion ratio, the accuracy of the undepleted regime approximation reduces and the difference between the analytical model and the measurements slightly increases as it is evident comparing Fig. 12(a) and Fig. 12(b). Nevertheless, the results in Fig. 11 and Fig. 12 clearly show that the difference between the analytical solution and the measurements is still negligible for 20% of depletion thanks to the high accuracy resulting from the steepest descent method for obtaining Eq. (12).

#248690 Received 31 Aug 2015; revised 14 Oct 2015; accepted 28 Oct 2015; published 3 Nov 2015

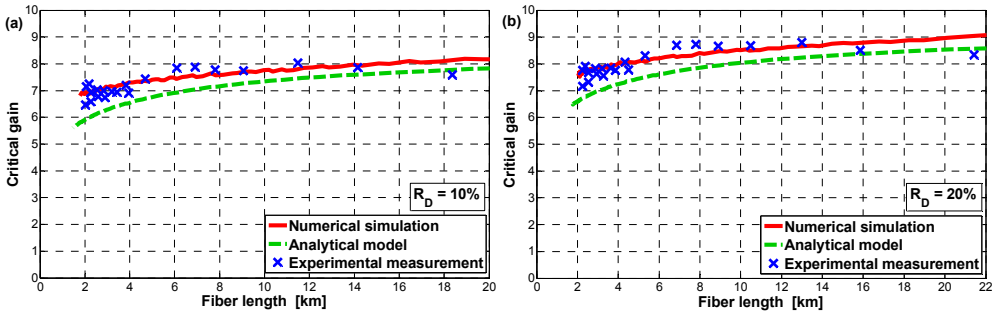

Fig. 12. Critical linear gain σ_{crit} versus fiber length for two depletion ratios: (a) R_D = 10% and (b) R_D = 20%; the plots compare measurements, simulations and results of the proposed analytical model.

5. Conclusion

In conclusion, a simple model for the critical power of modulation instability in optical fibers has been proposed and validated by experimental measurements and numerical simulations. The model can be used as a rule of thumb to avoid MI when designing fiber-optic systems, especially, long-haul optical communication networks and long-range distributed fiber sensors, completing with a similar simplicity the relations established long ago for SBS and SRS [38]. The MI gain spectrum in undepleted regime for lossless and lossy fibers has been investigated and their approximate analytical expressions have been compared to the exact numerical results in order to grant the accuracy of the model. The impact of background noise, mainly the ASE generated by EDFAs, has been considered in the model and verified experimentally, showing that the ASE level co-propagating with the signal has a great impact on the onset of modulation instability and thus the amount of MI-induced pump depletion. Furthermore, the FPU recurrence phenomenon has been observed based on the experimental measurements and numerical results, revealing that it only occurs in high depletion regime. The accuracy of the MI critical power and critical gain given in the analytical model has been experimentally demonstrated using Brillouin gain traces acquired using a BOTDA system. Results highlight that the model provides a nearly perfect solution for the evolution and critical parameters associated to modulation instability in optical fibers.

Appendix 1

In this appendix we derive the MI gain given in Eq. (2) based on the signal-idler approach utilized in OPA. Suppose f and h denote the signal and idler or the Stokes and anti-Stokes components around the pump frequency. Using the linear stability analysis it can be easily seen that the signal at fiber position L is given by $f(L) = f(0)A(L) + h^*(0)B(L)$ where $f(0)$ and $h(0)$ are initial values of the signal and idler. A and B are the signal and idler field gains given by [1,32]:

$$A(L) = \cos\mathrm{h}(gL) + i\frac{\gamma P_0 + \Delta\beta/2}{g}\sin\mathrm{h}(gL), \qquad B(L) = i\frac{\gamma P_0}{g}\sin\mathrm{h}(gL), \tag{19}$$

where P_0 is the input pump power, γ is the nonlinear coefficient, $\Delta\beta$ is the linear phase mismatch and g is the parametric gain coefficient given in Eq. (3). The signal gain G_S is obtained by imposing the initial conditions $f(0) = 1$ and $h(0) = 0$ on the field so that $f(L) = A(L)$ and thus:

$$G_S = |f(L)|^2 = |A(L)|^2 = 1 + \left(\frac{\gamma P_0}{g}\right)^2 \sin\mathrm{h}^2(gL). \tag{20}$$

#248690 Received 31 Aug 2015; revised 14 Oct 2015; accepted 28 Oct 2015; published 3 Nov 2015

On the other hand, the idler gain G_I is obtained by applying $f(0) = 0$ and $h(0) = 1$ on the field evolution leading to $f(L) = B(L)$ and therefore:

$$G_I = |f(L)|^2 = |B(L)|^2 = \left(\frac{\gamma P_0}{g}\right)^2 \sinh^2(gL). \quad (21)$$

For modulation instability the background noise plays the role of signal and idler, and so the initial conditions can be represented by random variables. Since the noise is assumed to be white the Stokes and anti-Stokes components have the same intensity that we set equal to unity here for calculating gains. However, they have random phases, i.e. $f(0) = e^{i\varphi}$ and $h(0) = e^{i\psi}$ where φ and ψ are independent random variables uniformly distributed over $[0,2\pi]$. In this case the field is given by $f(L) = e^{i\varphi}A(L) + e^{-i\psi}B(L)$ and its intensity is obtained as:

$$|f(L)|^2 = |A(L)|^2 + |B(L)|^2 + e^{i(\varphi+\psi)}A(L)B^*(L) + e^{-i(\varphi+\psi)}A^*(L)B(L). \quad (22)$$

The MI gain is obtained by the ensemble average of the field intensity. Since φ and ψ are independent and uniformly distributed over $[0,2\pi]$ it can be easily seen that the phase terms in Eq. (22) cancel out by averaging. Therefore, the MI gain expresses as follows:

$$G_{MI} = \mathrm{E}\left[|f(L)|^2\right] = |A(L)|^2 + |B(L)|^2 = G_S + G_I, \quad (23)$$

where E denotes the expected value. Equation (2) is the direct result of Eq. (23). In other words, since the initial idler and signal are white noises, their gains sum up incoherently.

Appendix 2

This appendix describes some mathematical details used to approximate the integral of the MI gain spectrum presented in Eq. (11). This integral is actually required to calculate the power inside the MI sidebands; and therefore, having a good approximation is essential to ensure a good accuracy of the proposed analytical model. To do this, the method of steepest descent [52], also called the saddle-point approximation, which is an extension of Laplace's method, has been used. This method is actually the same previously used for the calculation of the critical power of stimulated Raman and Brillouin scattering [38,56,57]. The following theorem describes how the method works.

Theorem: Consider the two non-exponential real functions $f(x)$ and $g(x)$ so that f has a sharp peak at x_0. For a positive variable s, the following approximation is held [52]:

$$I(s) = \int_{-\infty}^{+\infty} g(x)e^{s f(x)}dx \approx g(x_0)\mathrm{e}^{s f(x_0)}\sqrt{\frac{2\pi}{s|f''(x_0)|}}. \quad (24)$$

Proof: Since the rapidly varying term of the integral is the exponential function $e^{s f(x)}$, which has its maximum at x_0, the first approximation is to take the slowly varying function g out of the integral at point x_0, leading to:

$$I(s) \approx g(x_0)\int_{-\infty}^{+\infty} e^{s f(x)}dx. \quad (25)$$

Expanding the function f around x_0 using the Taylor series approximation and considering that $f'(x_0) = 0$, since x_0 is a maximum, we have:

$$f(x) \approx f(x_0) + f'(x_0)(x-x_0) + \frac{f''(x_0)}{2}(x-x_0)^2 = f(x_0) + \frac{f''(x_0)}{2}(x-x_0)^2. \quad (26)$$

This way the integral in Eq. (25) can be approximated as follow:

$$\int_{-\infty}^{+\infty} e^{s f(x)}dx \approx e^{s f(x_0)}\int_{-\infty}^{+\infty} e^{\frac{s f''(x_0)}{2}(x-x_0)^2}dx. \quad (27)$$

#248690 Received 31 Aug 2015; revised 14 Oct 2015; accepted 28 Oct 2015; published 3 Nov 2015

Since f has a maximum at x_0, $f''(x_0)$ is negative and hence the above integral is Gaussian and will converge to the following value:

$$\int_{-\infty}^{+\infty} e^{\frac{s f''(x_0)}{2}(x-x_0)^2} dx = \sqrt{\frac{2\pi}{s\left|f''(x_0)\right|}}. \tag{28}$$

Substituting the above expression in Eq. (25) gives the result in Eq. (24). ■

In order to use the above theorem, the following exponential approximation is first considered for the hyperbolic sine:

$$\sin \mathrm{h}^2(u) \approx \frac{e^{2u}}{4}, \qquad \text{for } u \gg 1. \tag{29}$$

In the neighborhood of $x_0 = \sqrt{0.5}$, where the gain has its peak and the approximate expression in Eq. (29) is valid, i.e. $u = \gamma P_0 L_{\text{eff}} >> 1$, the function $G_{\text{p}}(x)$ in Eq. (11) is given by:

$$G_{\text{p}}(x) = \frac{\sin \mathrm{h}^2\left(2\gamma P_0 L_{\text{eff}} \sqrt{x^2\left(1-x^2\right)}\right)}{2x^2\left(1-x^2\right)} \approx \frac{\exp\left(4\gamma P_0 L_{\text{eff}} \sqrt{x^2\left(1-x^2\right)}\right)}{8x^2\left(1-x^2\right)}. \tag{30}$$

Accordingly, the integration in Eq. (12) can be approximated as:

$$I = \int_0^{\infty} G_{\text{p}}(x)\, dx \approx \int_{-\infty}^{\infty} \frac{\exp\left(4\gamma P_0 L_{\text{eff}} \sqrt{x^2\left(1-x^2\right)}\right)}{8x^2\left(1-x^2\right)} dx. \tag{31}$$

Comparing Eq. (24) and Eq. (31) leads to the following substitutions:

$$\begin{cases} s = 4\gamma P_0 L_{\text{eff}} \\ f(x) = \sqrt{x^2\left(1-x^2\right)} \\ g(x) = \left(8x^2\left(1-x^2\right)\right)^{-1} \end{cases}, \tag{32}$$

where $x_0 = \sqrt{0.5}$, thus leading to $f(x_0) = 0.5$, $g(x_0) = 0.5$ and $f''(x_0) = -4$. Substituting these values in Eq. (24) results in the expression described in Eq. (12).

Acknowledgments

The authors would like to thank Simon Zaslawski for measuring the nonlinear coefficient of the optical fiber used in this work. Mehdi Alem appreciates fruitful discussions with Dr. Armand Vedadi. The authors also acknowledge the support from the Swiss Commission for Technology and Innovation through CTI Project 13122.1.

#248690 Received 31 Aug 2015; revised 14 Oct 2015; accepted 28 Oct 2015; published 3 Nov 2015